Insights into few-layer epitaxial graphene growth on 4*H*-SiC(000$\bar{1}$) substrates from STM studies

Laura B. Biedermann,[1,2] Michael L. Bolen,[3,2] Michael A. Capano,[3,2] Dmitry Zemlyanov,[2] and Ronald G. Reifenberger[1,2]
[1]*Department of Physics, Purdue University, West Lafayette, Indiana 47907, USA*
[2]*Birck Nanotechnology Center, Purdue University, West Lafayette, Indiana 47907, USA*
[3]*School of Electrical Engineering, Purdue University, West Lafayette, Indiana 47907, USA*
(Received 7 October 2008; revised manuscript received 21 January 2009; published 6 March 2009)

Epitaxial carbon was grown by heating (000$\bar{1}$) silicon carbide (SiC) to high temperatures (1450–1600 °C) in vacuum. A continuous graphene surface layer was formed at temperatures above 1475 °C. X-ray photoelectron spectroscopy (XPS) and scanning tunneling microscopy (STM) were extensively used to characterize the quality of the few-layer graphene (FLG) surface. The XPS studies were useful in confirming the graphitic composition and measuring the thickness of the FLG samples. STM studies revealed a wide variety of nanometer-scale features that include sharp carbon-rich ridges, moiré superlattices, one-dimensional line defects, and grain boundaries. By imaging these features with atomic-scale resolution, considerable insight into the growth mechanisms of FLG on the carbon face of SiC is obtained.

DOI: 10.1103/PhysRevB.79.125411 PACS number(s): 68.37.Ef, 81.05.Uw, 79.60.−i

I. INTRODUCTION

The production of high-quality materials with nanoscale size and reduced dimensionality is desirable for many advanced electronic applications. Materials such as two-dimensional (2D) graphene, one-dimensional (1D) carbon nanoribbons, and 1D carbon nanotubes represent a class of new materials that may well serve as the building blocks for future carbon-based nanoelectronics. Because of the reduced dimensionality of these emerging new materials, electron transport properties are expected to be strongly affected by disorder introduced by impurities, topological defects, or long-range deformation modes.[1] In nanomaterials, such disorder will cause unwanted quantum interference effects leading to increased scattering, unwanted localization, and an overall degradation in electronic performance. For this reason there is a pressing need to better characterize defects in any carbon-based nanomaterial.

A promising large area technique for graphene synthesis is to anneal in high vacuum a (000$\bar{1}$) silicon carbide (SiC) substrate to produce epitaxial carbon layers. Graphenelike sheets form in a complex process initiated by the sublimation of Si atoms and the formation of a carbon-rich surface containing mobile carbon atoms. Surface diffusion of carbon at elevated temperatures produces stacked sheets of planar six-fold coordinated carbon atoms.

A priori, it is possible to imagine a myriad of problems that may limit the quality of graphene layers that form on SiC. To begin, a high-quality SiC substrate is needed since a substrate surface full of step edges, localized defects, and microstructures will likely hinder atomic diffusion and thereby degrade the quality of the graphene layers formed. To obtain the highest quality single or bilayer graphene, a growth temperature that optimizes carbon atom diffusion with respect to Si atom sublimation must be determined. Because of the weak interaction between layers in stacked graphene, it is likely that shifts in atom stacking can develop between two adjacent graphene layers. To produce large areas of high-quality graphene, carbon grain boundaries must be reduced by both controlling and optimizing the number of C-rich seed regions. Identifying optimal growth conditions that (i) minimize the number of atomic-scale defects in a graphene sheet,[2] (ii) minimize the presence of grain boundaries,[3] and (iii) eliminate interstitial carbon atoms[4–8] between the graphene sheets presents a formidable challenge. Before fabricating high-quality graphene-based electronic devices on an industrial scale, many of these important questions must first be addressed.

Traditional surface characterization tools such as low-energy electron diffraction (LEED), Raman, and x-ray photoelectron spectroscopy (XPS) are capable of providing structural and chemical information spatially averaged across the carbon-rich SiC substrate at the millimeter length scale. Low-energy electron microscopy (LEEM) can provide structural information with a spatial resolution of ~10 nm. Atomic force microscopy (AFM) can provide useful topographic information for length scales ranging from tens of microns down to nanometers but cannot address local atomic or electronic structure. To obtain useful information about the quality of the carbon layers at the nanoscale, techniques capable of imaging individual carbon atoms are required. For this purpose, only scanning tunneling microscopy (STM) techniques seem suitable since STM techniques can reveal the atomic rearrangements produced by strains and defects as well as probe the local electronic properties of the graphene layers.

In what follows, we use ambient STM to characterize the atomic-scale structures found on epitaxial few-layer graphene (FLG) grown by heating (000$\bar{1}$) SiC to high temperatures (1450–1600 °C) in vacuum. Such a study is warranted since, historically, the C face is seldom studied because of the wide-spread use of the Si face in the production of SiC power devices.[9] By careful study of the atomic-scale STM images for different growth conditions, useful information about the quality of the FLG is obtained and valuable insights into the likely processes influencing the growth of graphene layers can be inferred.

II. SUPERLATTICES IN LAYERED CARBON

A. Defects in highly orientated pyrolitic graphite

The defects likely to occur in epitaxial graphene layers can be inferred from the extensive prior literature on highly orientated pyrolitic graphite (HOPG). Since the mid-1980s, STM has been used to extensively characterize defects in as-prepared HOPG that include (i) monolayer pits, step edges, stacking faults, and microholes,[10,11] (ii) pentagonal or heptagonal defective unit cells, (iii) the $\sqrt{3}\times\sqrt{3}$-$R30°$ superstructure caused by perturbation of the electronic charge density produced by point defects and adsorbed species,[12,13] (iv) 1D superlattices attributed to grain boundaries in HOPG,[14] and (v) moiré superlattices.[15–17]

Of particular interest to the current work are the high-quality moiré superlattices observed in STM images of HOPG surfaces.[15–17] The moiré superlattices on HOPG are characterized by a well-defined hexagonal superlattice with periodicities considerably larger than the atomic spacing between carbon atoms. Moiré regions observed on HOPG frequently have a sharp 1D transition, often described as a "string of beads,"[16] between the area supporting a superlattice and an adjacent area characterized by the 0.246 nm atomic periodicity of HOPG. The beadlike features demarcating the sharp boundary between the two regions typically have the same periodicity as the superlattice.[17]

The presence of moiré superlattices on HOPG is usually attributed to the rotation of the top graphene sheet with respect to the second layer, which can result from purely mechanical means.[16,18] In the case of a rotation, the moiré superlattice has a constant periodicity across the moiré region. Alternatively, a screw dislocation can cause a gradual rotation of the top graphene layer in HOPG; the superlattice periodicity around such a dislocation continuously varies with distance.[17] While the origins and manifestations of these superlattices on HOPG are interesting in their own right, the observation of moiré superlattices on FLG grown epitaxially on SiC is relatively new.[19]

B. Superlattices in FLG

Two types of superlattices have been reported on epitaxial graphene formed on a SiC substrate. First, if the graphene layer is only one or two monolayers thick, the SiC substrate reconstruction can be observed using STM, LEED, or surface x-ray diffraction (SXRD).[20–27] As observed by STM and LEED studies of Si-face graphitized SiC, this reconstruction is manifested as a 6×6 or a $(6\sqrt{3}\times6\sqrt{3})R30°$ structure.[28–31] By contrast, the C-face reconstructions are not as well studied; Hass *et al.*[32] reported a $(\sqrt{13}\times\sqrt{13})R46.1°$ superlattice on $4H$-SiC$(000\bar{1})$ with STM.

A second type of superlattice formed on FLG is a moiré superlattice due to the rotation or dislocation of the top graphene layers. Such superlattices were recently reported on epitaxial graphene by Varchon *et al.*,[19] who found six distinct moiré regions within a 150×150 nm^2 STM scan with periodicities ranging from 2.5 to 3.8 nm. The separate moiré regions were bounded by either ridges (called pleats by Varchon *et al.*[19]) or a "string of beads." To be complete, it is worth noting that dilation moiré superlattices are also observed on chemical vapor deposition (CVD) grown graphene on substrates such as Ir(111), Ni(111), Ru(0001), and Pt(111).[33–36] In this case, the superlattice is attributed to differences between the lattice constants of the graphene and substrate and not to a rotation between graphene layers.

C. Atomic arrangement of moiré superlattices

The origin of the moiré superlattices is an enhancement in the density of states (DOS) which occurs when the topmost layer of graphene is rotated with respect to the underlying layer(s), resulting in a range of possible atomic arrangements.[37] This rotation results in three key graphite stacking sequences, **BAB**, **AAB**, and **slip B**.[16] The standard Bernal arrangement is **BAB** stacking. In **AAB** stacking, each atom in the top layer is directly above an atom in the next lower layer. An intermediate case is referred to as the **slip B** stacking. In this case, the **BAB** stacking is offset slightly such that no atom in the top layer is directly above an atom in the next lower layer.

Using density-functional calculations, Campanera *et al.*[37] found that the moiré superlattices observed by STM could be replicated using four layers of **BA**-stacked graphite, where the top layer was rotated with respect to the bottom layers. The brightest features observed in STM images of the moiré superlattices correspond to the **AAB** stacking, which was found to have the highest DOS. Dim features correspond to the **slip B** stacking, while the darkest features correspond to the standard **BAB** Bernal stacking of HOPG. Furthermore, Campanera *et al.*[37] calculated a relative formation energy cost of a few meV/atom, with a higher-energy cost corresponding to larger observed periodicities.

The superlattice periodicity can be characterized by a length $\mathcal{D}$ given by

$$\mathcal{D} = \frac{a}{2\sin(\Theta/2)}, \tag{1}$$

where a is the basal lattice constant (0.246 nm for HOPG) and Θ is the rotation angle between two layers of the hexagonal lattice. The orientation of the moiré lattice with respect to the atomic orientation of the top graphene layer is given by ϕ, where[17]

$$\phi = 30° - \Theta/2. \tag{2}$$

As evident from Eq. (1), a small rotation angle, Θ, corresponds to a large superlattice periodicity, $\mathcal{D}$.

It is important to note that the moiré superlattices are atomically flat; the apparent enhanced corrugation is a DOS effect. The presence of moiré superlattices implies that electrons in FLG traversing a region containing the superlattice are subjected to an additional potential with a periodicity $\mathcal{D}$. Since the moiré superlattice is a DOS effect, the prominence of this superlattice depends on the bias voltage and tunneling current. The moiré superlattice is most prominent when the STM tip is closest to the sample, which corresponds to small bias voltage and large tunnel currents.

III. EXPERIMENTAL CONSIDERATIONS

A. Graphene growth

4*H*-SiC wafers (Cree, high purity and semi-insulating) with 3 in. diameter and a nominal off-cut angle of 0° were used throughout this study. The as-received SiC wafers were polished by NovaSiC to remove scratches and other surface defects. The wafers were then diced into 8×8 mm^2 substrates and cleaned.

The FLG samples were grown on the carbon face of the SiC$(000\bar{1})$ substrates in an Epigress VP508 hot-wall chemical vapor deposition reactor. The temperatures reported in this study were determined using a Heitronics KT81R two-color rationing pyrometer (spectral bands 0.7 and 1.2 μm) with a calibration traceable to the melting temperature of Si (1410 °C).

Prior to carbon growth, the SiC substrates were hydrogen annealed at 1600 °C to etch residual polishing damage. The temperature was reduced to 700 °C and the pressure was reduced to 2×10^{-7} mbar. The temperature was then ramped up to a growth temperature between 1475 and 1600 °C to form continuous carbon layers. The SiC substrate was held at the growth temperature for 10 min before the sample was cooled under vacuum[38] and prepared for characterization by XPS and STM.

B. XPS considerations

The XPS data were obtained with a Kratos Ultra DLD spectrometer using monochromatic Al Kα radiation ($h\nu$ =1486.58 eV). Survey and high-resolution spectra were collected at fixed analyzer pass energies of 160 and 20 eV, respectively. The spectra were collected at 0°, 30°, 45°, 52°, and 60° with respect to the surface normal (photoemission angle θ). All binding-energy (BE) values refer to the Fermi level. The charge shift was corrected to the C 1*s* peak set at 284.5 eV for the graphitic component.[39] The standard deviation of the peak position associated with the charge reference procedure was ±0.05 eV. The data were analyzed with commercially available software, CASAXPS (version 2313Dev64). The spectra were fitted by a Gaussian-Lorentzian function after linear or Shirley-type background subtraction.

C. STM considerations

Ambient STM scans were performed using a Nanotec Electronica STM. The scans were performed under a bell jar that was backfilled with dry nitrogen to atmospheric pressure. The *X*, *Y*, and *Z* piezos were calibrated using the known atomic lattice (0.246 nm) and monostep height (0.335 nm) of HOPG. Typical scan parameters included a 0.1–5 nA tunnel current (I_{set}) and a bias voltage of 0.05–5 V (V_{bias}). STM scan sizes ranged from 2×2 nm^2 to 5×5 μm^2. Typical image acquisition times ranged from 30 s to 10 min. All STM scans presented were obtained in the constant current mode using a cut PtIr tip. Nanotec Electronica's WSXM software program was used for both data acquisition and image processing.[40]

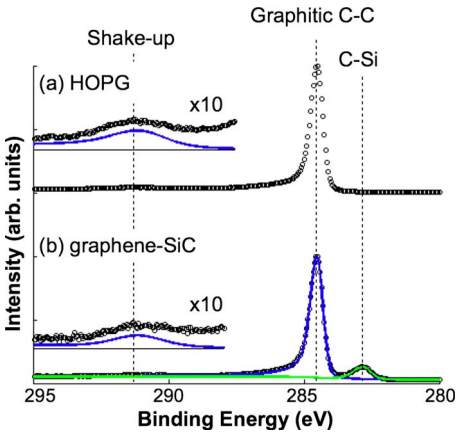

FIG. 1. (Color online) The C 1*s* XPS spectra, collected at θ =0°, (a) from a reference HOPG substrate and (b) from a FLG sample grown at 1500 °C on SiC. The similarity of the two XPS spectra indicates the presence of graphitic carbon on SiC. Both spectra were obtained at a photoemission angle of 0°. A closer examination of the region between 288 and 295 eV from both samples provides evidence for shake-up satellites (insets).

IV. XPS CONFIRMATION OF GRAPHITIC CARBON AND ESTIMATION OF GRAPHENE THICKNESS

Systematic angle-resolved XPS studies were performed on FLG samples. Of prime interest were confirmation of graphene growth and a nonintrusive estimate of FLG thickness. For this reason, we focus on the FLG samples grown at 1475 and 1500 °C. Figure 1 shows an example of the C 1*s* core-level spectrum obtained from a FLG sample grown at 1500 °C; the spectrum from a reference HOPG sample is shown for comparison as well. The spectra from both HOPG and the 1500 °C FLG sample show a main peak at 284.5 eV, indicating the presence of sp^2 hybridized C-C bonds. This peak at 284.5 eV is a signature of graphitic carbon.[41] The small peak at 283.0 eV in the XPS spectrum from the graphene-SiC sample is assigned to carbon bound to silicon.[41,42]

Another signature of graphitic carbon is a weak peak at approximately 291 eV, which is identified as a shake-up satellite of the peak at 284.5 eV. The shake-up satellite is a well-established characteristic of the photoemission process in aromatic and graphitic systems.[43] The shake-up is a two electron phenomenon; the emitted photoelectrons with energy 284.5 eV can excite a $\pi\rightarrow\pi^*$ transition resulting in an additional peak at higher BE. Aromatic and graphitic systems show a shake-up peak shifted toward higher BE from the main peak by approximately 6.5–7 eV with an intensity ranging up to 5%–10% of the graphitic peak.[43]

In order to estimate the thickness of the graphitic carbon from XPS data, we utilized the approach proposed by Fadley.[44] Assuming the graphene-SiC sample can be modeled as a semi-infinite SiC substrate with a uniform graphene overlayer of thickness t, t can be calculated from the ratio between the intensity of the graphitic component at 284.5 eV from the graphene overlayer, $N_G(\theta)$, and the intensity of the SiC component at 283.0 eV from the SiC substrate, $N_{SiC}(\theta)$:

$$\frac{N_G(\theta)}{N_{\mathrm{SiC}}(\theta)} = \frac{\rho_G \Lambda_e^G(E_{\mathrm{C}\,1s})}{\rho_{\mathrm{SiC}} \Lambda_e^{\mathrm{SiC}}(E_{\mathrm{C}\,1s})} \left\{ \frac{1 - \exp\left[\frac{-t}{\Lambda_e^G(E_{\mathrm{C}\,1s})\cos\,\theta}\right]}{\exp\left[\frac{-t}{\Lambda_e^G(E_{\mathrm{C}\,1s})\cos\,\theta}\right]} \right\}. \tag{3}$$

Here ρ_G and ρ_{SiC} are the densities of carbon atoms in graphene and SiC in atoms per cm^3, respectively. Λ_e^G and Λ_e^{SiC} are the attenuation lengths for the C 1*s* photoelectron with kinetic energy $E_{C\,1s}$. The quantities $\Lambda_e^G = 3.10$ nm and $\Lambda_e^{\mathrm{SiC}} = 2.58$ nm were calculated using NIST SRD-82 (Ref. 45); details of this calculation and the derivation of Eq. (3) are explained in the supporting information.[46] The peak intensities $N(\theta)$ also depend on physical parameters of the spectrometer and electron analyzer, but these parameters are the same for both $N_G(\theta)$ and $N_{\mathrm{SiC}}(\theta)$ and thus cancel.

The XPS spectra can be fit by two components, as shown in Fig. 1, and the ratio between the graphene and SiC components, $N_G(\theta)/N_{\mathrm{SiC}}(\theta)$, can be accurately measured. Since $N_G(\theta)/N_{\mathrm{SiC}}(\theta)$ was measured over a range of θ between 0° and 60°, a least-squares fit to Eq. (3) was used to determine *t*. For more information on the thickness calculation, please see the supplementary information.[46] Since the XPS spot size is 0.4×0.7 mm^2, the thickness estimate represents an average value characterizing the FLG thickness across a few hundreds of microns. In this way, the average thickness of the FLG grown at 1500 °C was found to be 2.4 ± 0.2 nm or approximately 7 monolayers (ML) of graphene. Using the same XPS analysis method, the average thickness of the FLG grown at 1475 °C was found to be 1.8 ± 0.1 nm or approximately 5 ML of graphene. These thickness values provide a convenient benchmark to qualitatively estimate the thickness of FLG formed at different growth temperatures.

V. STM RESULTS

In what follows, we discuss in turn the nanoscale features that have been found on FLG using STM. These features are useful for providing insight into graphene growth.

A. General observations

AFM studies[47] show the SiC substrate (carbon face) to be stepped, with flat terraces a few hundred nanometers wide. The terraces are terminated by steps ranging in height from ~0.7 nm to ~2 nm. The flat terraces occasionally show rough features, presumably due to inadequate chemomechanical polishing.

A wide growth temperature range, 1450–1600 °C, was investigated to better understand the growth mechanisms of graphene on SiC. Parallel XPS and AFM studies[47] provided evidence that at temperatures below 1475 °C, the carbon coverage was sufficiently sparse that continuous FLG was not formed. The samples grown at these lower temperatures were not extensively studied by STM since the low electrical conductivity of the exposed SiC substrate led to an unstable tunnel current. Occasionally, large pits (~0.3–1.0 μm wide) surrounded by multiple graphene ridges were found.

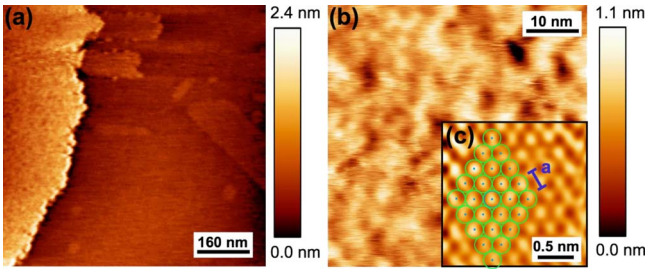

FIG. 2. (Color online) STM images of graphene grown at 1475 °C shows the two growth morphologies. In (a), an 800×800 nm^2 region, the rough graphene region is on the left while the smooth graphene region is on the right. In (b), a 50×50 nm^2 image showing the detailed morphology of the rough graphene. In (c), a 2×2 nm^2 atomic-resolution image of the rough region in (b) reveals a hexagonal lattice. The lattice parameter $a = 0.245$ nm of the hexagonal lattice indicates the presence of graphene. The original STM scan was processed with wavelet analysis (Ref. 49). Scan parameters are $I_{\mathrm{set}} = 5.0$ nA and $V_{\mathrm{bias}} = 72$ mV for (a) and $I_{\mathrm{set}} = 3.0$ nA and $V_{\mathrm{bias}} = 100$ mV for (b) and (c).

These defects were rare and are thought to be formed from screw or edge dislocations in the SiC substrate. It is likely that the hydrogen etching procedure enhanced these defects.[48] These substrate defects will not be discussed further, as all STM scans presented were taken away from such pits.

B. Rough graphene

At growth temperatures of 1475 °C, smooth graphenelike surfaces of $t = 1.8 \pm 0.1$ nm (XPS measurement) allowed reliable and reproducible STM studies. The graphene that formed at this growth temperature showed two morphologies that we name smooth graphene and rough graphene. An STM image of these two regions is provided in Fig. 2(a). A step edge of 1.4 nm separates the smooth and rough regions. The smooth graphene, as confirmed by atomic-resolution scans, was atomically flat and provided evidence for monolayer C step heights of 0.3 nm. The rough graphene had a rms roughness of typically 0.15–0.20 nm and showed peak to valley heights of ~0.2–0.5 nm [Fig. 2(b)]. In spite of the roughness, it was possible to obtain atomic-resolution scans over small 4–10 nm^2 regions. Fast Fourier transforms (FFTs) of atomic-resolution scans yielded a hexagonal periodicity of 0.22 ± 0.01 nm, indicating the presence of graphene.

We find evidence for grain boundaries in rough graphene formed at a growth temperature of 1500 °C ($t = 2.4 \pm 0.2$ nm, XPS measurement). This is illustrated in Fig. 3(a) which shows a grain boundary separating two regions of rough graphene. The width of the boundary is ~50 nm. A more detailed STM image of the boundary region is provided in Fig. 3(b). This figure shows randomly oriented parallel 1D features with a periodicity of ~4 nm. These localized, 1D features have only been observed in the rough graphene regions of the substrate.

C. 1D superlattice on smooth FLG

We have observed 1D superlattices that cut across smooth regions of FLG. An example of such a defect on sample 2,

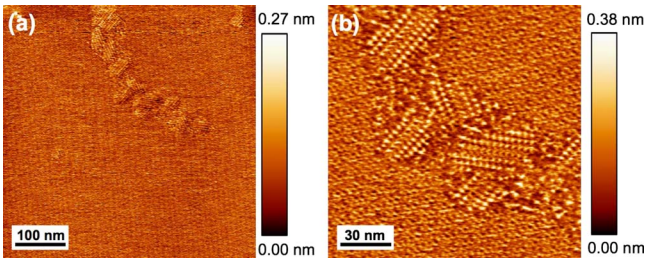

FIG. 3. (Color online) STM images of a region from the graphene grown at 1500 °C. In (a), a 500×500 nm^2 image showing the presence of a grain boundary in the upper half of the image. In (b), a 150×150 nm^2 image showing the parallel 1D features within the grain boundary. Scan parameters are $I_{set}=2.0$ nA and $V_{bias}=100$ mV for (a) and (b).

grown at 1500 °C, is shown in Fig. 4(a). Two fiducial lines *AB* and *CD* are drawn parallel to each other. The resulting angles between the fiducial lines are $\angle ABC=141°\pm5°$ and $\angle CDE=136°\pm5°$, indicating that the 1D superlattice is bent from a straight line by an average angle of about $42°\pm5°$. The periodicity of the 1D superlattice is well defined and equal to 7.0 nm between points *A* and *B* [see Fig. 4(b)]. This 1D feature resembles a 1D moiré superlattice reported on HOPG that contained a 30° bend and was attributed to a grain boundary in the graphene layer.[14]

D. Ridges on FLG

At growth temperatures of 1500 °C, the FLG ($t=2.4\pm0.2$ nm, XPS measurement) exhibited atomically smooth surfaces across large regions of the underlying SiC substrate. In addition, fine ridgelike features, up to ~10 nm tall, begin to form boundaries around the atomically smooth FLG domains. In many cases, the ridges cross step edges in the underlying SiC substrate with no change in height or direction [see Fig. 5(a)]. Occasionally, ridges form on step edges, as is the case for the 6-nm-high ridge, which is located on a 4.5 nm step edge [see Fig. 5(b)]. The formation of a ridge that exactly follows a step edge suggests that step edges in the underlying SiC substrate might provide a diffusion barrier to mobile carbon atoms at 1500 °C. As the growth temperature increases beyond 1500 °C, the ridges appear to coalesce into much taller and wider folds (up to

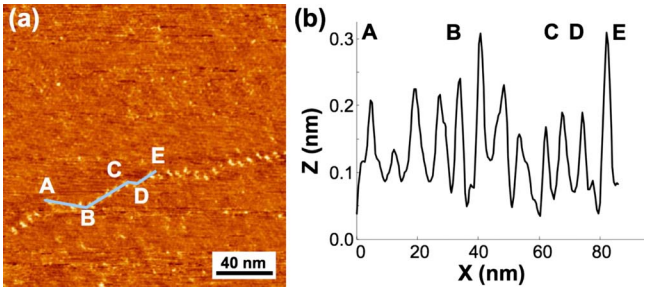

FIG. 4. (Color online) (a) An STM image of a 200×200 nm^2 region shows a 1D superlattice. (b) A line profile along the line *ABCDE*, which follows the profile of the 1D superlattice. Scan parameters are $I_{set}=2.0$ nA and $V_{bias}=300$ mV.

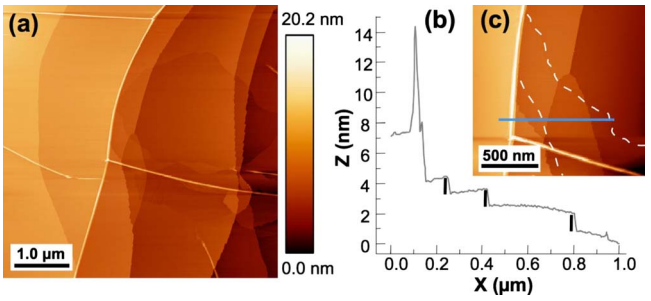

FIG. 5. (Color online) (a) An STM image of a 5×5 μm^2 region shows fine ridges, 5–10 nm high, crossing the sample. (c) A 1.5×1.5 μm^2 region located in the center of (a) reveals a superlattice, the boundaries of which are indicated by the dashed lines. This superlattice is bounded by the ridge on the left-hand side and is discussed further in Fig. 7. A profile (b) across (c) shows a 6-nm-high and 40-nm-wide ridge. Steps in the underlying SiC substrate are indicated by vertical black bars (1.1 nm tall). Scan parameters are $I_{set}=5.7$ nA and $V_{bias}=72$ mV for (a) and $I_{set}=1.0$ nA and $V_{bias}=300$ mV for (c).

~20 nm high) that form boundaries encompassing larger areas of smooth FLG. STM $I(V)$ measurements on the ridges show a linear behavior that is indistinguishable from $I(V)$ data acquired on the nearby flat regions of the FLG. Frequently, the ridges intersect with angles near ~120° (not shown). These ridges of graphene are thought to be caused by the thermal expansion mismatch between graphene and SiC.[32,47] Similar ridges are observed on CVD-graphene grown on Ni.[34]

E. Moiré superlattices on FLG

Moiré superlattices were observed on 4*H*-SiC$(000\bar{1})$ FLG samples grown at 1500 and 1550 °C. Interestingly, no moiré superlattices were observed on samples grown at either 1475 or 1600 °C. An example of a moiré region is provided in Fig. 5(c) (growth temperature of 1500 °C). These superlattices were confined to regions adjacent to ridges; the superlattices were found either on one or both sides of the ridge. It was often observed that the FLG regions adjacent to the ridges were no longer flat but exhibited a pronounced curvature that persisted over ~0.5 μm distance from the ridge. Superlattices were never found as isolated islands surrounded entirely by a flat FLG region. By randomly sampling well-separated regions of the FLG surface, moiré regions with different superlattice periodicities were found at different positions across the same FLG sample. These results are summarized in Table I, which indicates that periodicities of the superlattices from three FLG samples range between 4 and 13 nm.

F. Atomic resolution within a moiré superlattice

Atomic-resolution STM images of a moiré superlattice are given in Figs. 6(a) and 6(c). Distinct regions of apparently different heights are clearly visible as dark, dim, and bright areas. As a guide to the eyes, two lines are drawn on top of the STM image; the dashed line follows the superlat-

TABLE I. Samples with moiré superlattice patterns and their measured periodicity.

Sample	Growth temperature (°C)	$\mathcal{D}$ (nm)	Θ (deg)
1	1500	5.6 ± 0.3	2.5 ± 0.1
2	1500	4.2 ± 0.2	3.3 ± 0.1
		4.7 ± 0.3	3.0 ± 0.2
		9.4 ± 2.2	1.5 ± 0.3
		12.7 ± 2.1	1.1 ± 0.2
3	1550	6.4 ± 0.7	2.2 ± 0.3
		7.2 ± 0.5	2.0 ± 0.2
		9.0 ± 0.6	1.6 ± 0.1

tice bright areas while the solid line follows the atomic lattice of the carbon atoms.

By resolving the atomic positions in the FLG layer, two independent ways of determining the relative rotation angle of the top graphene layer with respect to the underlying layers become possible. First, using the measured periodicity of the superlattice from the 2D-FFT [4.44 ± 0.31 nm in Fig. 6(b)], the angle $\phi = 28.4 \pm 0.2°$ can be calculated from Eqs. (1) and (2). Second, the angle can be measured directly from the atomically resolved STM image in Fig. 6(a), giving a value of $\phi = 26 \pm 2°$. These two results are in good agreement with each other. As indicated by the fiducial lines in Figs. 6(b) and 6(d), the same relative rotation, ϕ, observed in Fig. 6(a) is seen between the Fourier components in the superlattice scale and atomic-scale 2D-FFTs.

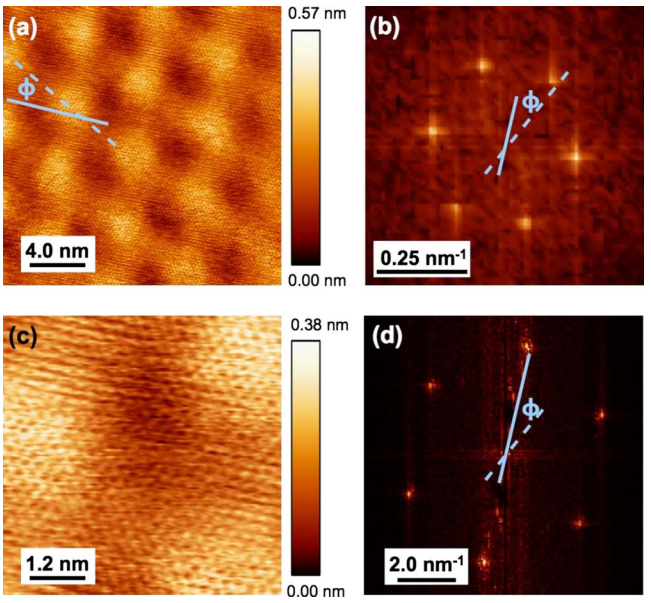

FIG. 6. (Color online) (a) An STM image of a 20×20 nm^2 region shows a moiré superlattice. (b) The 2D-FFT of the moiré superlattice shows the hexagonal superlattice ($\mathcal{D} = 4.44 \pm 0.31$ nm). Image (b) is a 2D-FFT of a 60×60 nm^2 region; the larger image is necessary for a high-resolution FFT. (c) A 6×6 nm^2 zoom of (a) shows the hexagonal lattice of the top graphene layer. (d) From the 2D-FFT of (a), the atomic lattice is found to be 0.23 ± 0.09 nm, close to the accepted value of 0.246 nm. The scale bars in (b) and (d) are the length of the k vector where $1/k$ is the lattice periodicity. Scan parameters are $I_{set} = 5.7$ nA and $V_{bias} = 72$ mV.

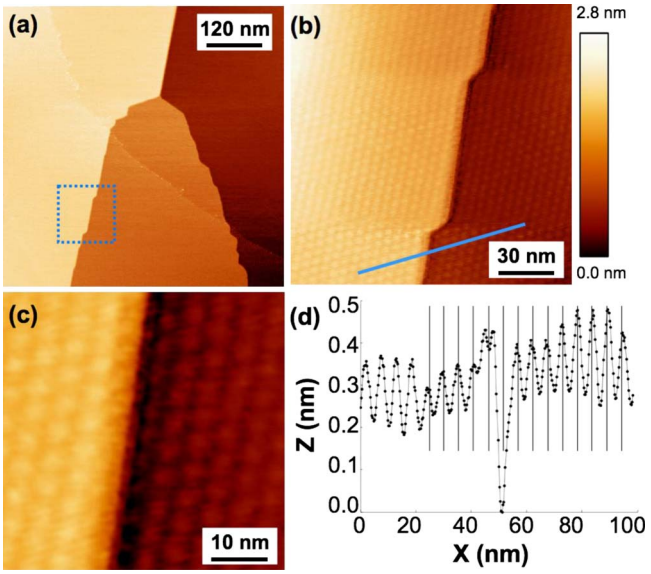

FIG. 7. (Color online) (a) An STM image of a 600×600 nm^2 region shows a moiré superlattice continuing across two step edges (both 1.1 nm high) in the SiC substrate. The dashed box in (a) indicates the 150×150 nm^2 region in (b), which was scanned at a higher resolution. The superlattice is clearly visible in (c), a 50×50 nm^2 magnified region of the center of (b). A profile (d) drawn across the step edge in (b) illustrates that no apparent row of atoms is missing at the step edge. To enhance the apparent periodicity, the height of the step edge was subtracted from this profile. Scan parameters are $I_{set} = 1.0$ nA and $V_{bias} = 300$ mV for (a) and $I_{set} = 1.5$ nA and $V_{bias} = 50$ mV for (b) and (c).

G. Moiré superlattice across a SiC step edge with constant periodicity $\mathcal{D}$

The long lateral range over which the moiré superlattices were observed permits an exquisitely sensitive way to map carbon atomic positions across localized defects such as a step edge in the underlying SiC substrate. One such example is illustrated in Fig. 7(a) which is an image from the FLG sample 2 grown at 1500 °C. In Fig. 7(b), the superlattice is observed to persist across a 1.1 nm step edge associated with the SiC substrate.

The measured periodicity of the superlattice in Fig. 7(b) was determined to be $\mathcal{D} = 4.7 \pm 0.3$ nm. In Fig. 7(d), the phase of the superlattice is tracked across the step edge. This topography profile illustrates that the superlattice exhibits a constant value of $\mathcal{D}$ and remains in phase as it traverses the step edge, indicating that the relative rotation between the top two layers of graphene is constant across the step. The observation of a commensurate moiré superlattice spanning a step edge in the substrate supports the suggestion that FLG growth follows a carpetlike growth mechanism proposed by Seyller *et al.*[50]

H. Termination and energetics of a small moiré region

Typically, the moiré regions in the FLG grown samples studied were large enough that the entire pattern could not be

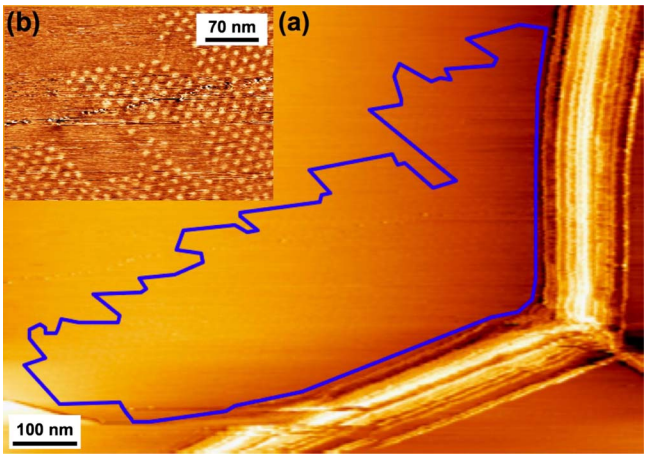

FIG. 8. (Color online) (a) An STM image (1000×700 nm^2) shows the extent of the moiré region with a periodicity of $\mathcal{D}=12.7\pm2.1$ nm, as indicated by the solid line. The exceptionally jagged edge of the moiré region is illustrated by the 350×250 nm^2 inset. Scan parameters are $I_{set}=1.0$ nA and $V_{bias}=300$ mV for (a) and $I_{set}=2.0$ nA and $V_{bias}=100$ mV for (b).

imaged within a single scan of dimension 1×1 μm^2. While larger STM scans are possible, the decreased lateral resolution obscures the moiré superlattice [cf. Figs. 7(a) and 7(b)]. An unusually small moiré region that could be imaged in a single STM scan was found on sample 2, which was grown at 1500 °C. This superlattice is characterized by a periodicity $\mathcal{D}=12.7\pm2.1$ nm and spans an area of 2.3×10^5 nm^2. As shown in Fig. 8(a), this moiré region is bordered by two tall ridges (8–10 nm high) located on the right and bottom of the image.

While the boundaries between moiré regions and Bernal stacked (**BAB**) graphene are rarely straight, the boundary of this superlattice is unique for the number of jagged protrusions it reveals [see Fig. 8(b)]. The ragged termination of the superlattice suggests that the relative rotation between the top two layers of graphene is relaxed by local defects in one of the two layers. The origin of the superlattice is likely high strain fields produced during ridge formation. Evidently the graphene lattice relaxes away from the ridge, causing the superlattice to disappear. The moiré periodicity remains constant up to the superlattice boundary, indicating that the graphene lattice does not appear to be stretched or otherwise distorted.

The minimum relative formation energy of a moiré superlattice is calculated to be 2.5 meV/atom.[37] At the 1500 °C growth temperature, the thermal energy per atom confined to 2D, k_BT, is 0.15 eV, where k_B is the Boltzmann constant. At this growth temperature, there is more than sufficient thermal energy to anneal this rotational defect if the rotation occurs at 1500 °C. This suggests the rotational defect is pinned by an energy barrier that requires significantly more than thermal energy before the rotational defect is relaxed. If the rotation occurs while the FLG sample is cooling, there may not be sufficient thermal energy to anneal the defect. Since the moiré regions are predominately found near ridges, it seems likely that the formation of a ridge causes a rotation of a few graphene layers, resulting in a moiré superlattice that is both created and pinned by the upward lift of individual graphene layers during the ridge formation.

I. Moiré superlattices coexistent with wavelike features

Wavelike features or ripples with a height of about 1 nm have been reported in TEM images of suspended exfoliated graphene sheets[51] as well as in STM studies of graphene.[52,53] The existence of ripples has implications for charge transport since curved regions of graphene are expected to modify the local density of electron states due to a potential that develops that is proportional to the square of the local mean curvature.[54–56] The precise origin of these ripples, with a focus on the structural integrity of a 2D graphene membrane, has been extensively discussed.[57–63]

We find evidence for rippling in FLG grown on SiC as shown in Fig. 9(a), on sample 3, grown at 1550 °C. The ripplelike features emanate from a 1-nm-high line defect and are aligned roughly perpendicular to this line defect. The ripples are approximately parallel to each other with a height of 0.1–0.2 nm and an apparent width of 20–50 nm [see Figs. 9(b) and 9(d)]. The ripples continue across a 0.65 nm step edge in the substrate. While usually found on flatter regions of FLG, a moiré superlattice has also been observed on this rippled region. A superlattice with an area of ~500

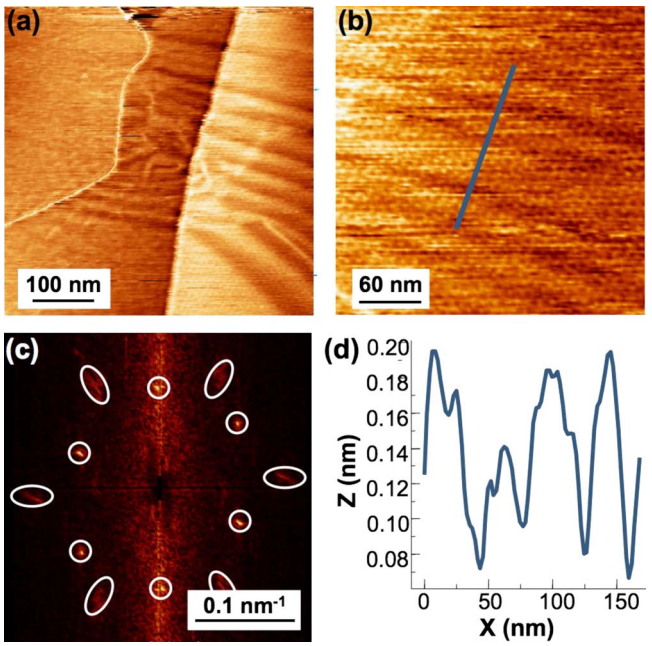

FIG. 9. (Color online) (a) An STM image, 500×500 nm^2, shows a 1-nm-high line defect that runs parallel for ~200 nm of its length to a 0.65 nm step edge. Carbon ripples emanate from the line defect and are found to cross over the step edge. In (b), an STM image of a 300×300 nm^2 zoom of the rippled region of (a) reveals that the superlattice is coexistent with the ripples. In (c), the hexagonal periodicity of the superlattice is confirmed by a 2D-FFT of (b). The superlattice is a superposition of two moiré patterns, with periodicities of $\mathcal{D}=9.3\pm1.2$ nm (bright inner spots) and $\mathcal{D}=6.4\pm0.7$ nm (dim outer spots). In (d), a profile of the ripples along the straight blue line in (b). Scan parameters are $I_{set}=1.0$ nA and $V_{bias}=500$ mV.

$\times 1000$ nm^2 floods the surface spanning the ripples. This superlattice is not disrupted by the ripples in the FLG surface.

Careful analysis of the FFT from Fig. 9(a) shows that the superlattice is actually a superposition of two moiré superlattices, implying that at least the top two, if not more, graphene layers are rotated with respect to each other. The relevant FFT is given in Fig. 9(c) and shows one periodicity with $\mathcal{D}=9.3$ nm and $\Theta=1.5°$ [highlighted by white circles in Fig. 9(c)], corresponding to the bright inner hexagonal pattern in the FFT. A second moiré superlattice [highlighted by white ellipses in Fig. 9(c)] is characterized by FFT spots that are dimmed and blurred slightly but is still clearly resolved. The periodicity and rotation of this second superlattice are measured to be $\mathcal{D}=6.4$ nm and $\Theta=2.2°$.

VI. IMPLICATIONS FOR EPITAXIAL GRAPHENE GROWTH ON SiC

Taken together, the results of the STM studies presented above are consistent with a nonuniform and heterogeneous environment for the growth of FLG on 4*H*-SiC$(000\bar{1})$ substrates. *A priori*, there are many reasons why a spontaneous and unseeded growth of a truly uniform and perfectly periodic FLG layer over an area larger than a few square micrometers of a 4*H*-SiC$(000\bar{1})$ substrate might be difficult to achieve. First, the basal plane lattice constant of graphene is ~30% smaller than SiC. As a consequence, in one layer of SiC, there are 12.2 C atoms/nm^2. To form one layer of graphene, 38.2 C atoms/nm^2 are required. Therefore, to free enough C atoms to form a continuous layer of graphene requires the sublimation of more than three layers of SiC.[26,32] Second, it is reasonable to expect that graphene growth nucleates at many sites across the SiC wafer. Last, there is a mismatch in thermal expansion between graphite and SiC. Our STM data provide evidence which suggests that all these issues hinder uniform graphene growth.

It is likely that the growth of FLG nucleates at step edges or terrace defects on SiC. Our studies show that at growth temperatures of 1475 °C, any localized patches of FLG that form on the C face of SiC have already merged to completely cover the SiC substrate. The observation of rough graphene in FLG could reflect a deficit in the supply of C atoms required to form a continuous layer of graphene. Owing to its random nature, sublimation is an uncontrollable process on the atomic scale that inherently roughens the substrate surface. Since the sublimation of more than three layers of SiC is required to free sufficient carbon to form one continuous graphene layer, it is likely that for the thinnest layers of FLG, the underlying roughness created by the uneven evaporation of the SiC substrate seeds the rough graphene growth. Compounding this stoichiometric issue is the reported rapid oxidation rate of the C face.[64] Oxidation of the SiC surface might also significantly contribute to the roughening of the first few layers of graphene. XPS data show that the presence of SiO_2 decreases as the growth temperature increases from 1475 to 1550 °C.

The presence of grain boundaries between advancing graphene layers might be anticipated if graphene growth is heterogeneously seeded across the SiC substrate. Indeed, we find evidence in the top FLG layer of 1D boundaries separating two graphene regions (see Fig. 4). The presence of these boundaries suggests that graphene sheets, seeded at different nucleation sites across the SiC substrate, do not always uniformly merge into one continuous graphene layer. An alternative explanation for the 1D boundaries is the formation of pentagonal or heptagonal defects during graphene growth, causing local buckling of the FLG.

As the growth temperature increases, we observe a transition between rough graphene layers (seen regularly at 1475 °C) to uniform atomically smooth FLG having an atomic periodicity identical to HOPG (seen regularly at 1550 °C). The increase in temperature increases the rate of Si sublimation, which occurs most rapidly at step edges, thereby providing more free carbon atoms. The higher growth temperature also increases the surface carbon atom mobility. As a consequence, at higher temperatures, thicker graphene films form with carbon atoms more readily forming sp^2 bonds, thus mitigating the surface roughness inherent at the SiC-graphene interface. Both the greater number of available carbon atoms and the increase in mobility contribute to the atomic smoothing of the graphene film.

As smooth FLG forms, our STM studies suggest that both 1D ridges and moiré superlattices develop. It is likely that the ridges form due to the difference in thermal contraction between the basal plane of graphite and the SiC substrate.[47] The exact location of a ridge could be seeded by lines of defects in the FLG layer. Based on $I(V)$ data, we have evidence that the 1D ridges (see Fig. 5) are as conducting as the surrounding flatter regions, suggesting that the ridges are graphitic. The height of the ridges is found to increase with the graphene layer thickness. Two ridges often intersect at a point, forming a subtended angle near 120°.

While ridges frequently traverse 1–2 nm high step edges at random angles, the ridges can also be aligned along step edges in the SiC substrate, such as the ridge parallel to the 4.5 nm step edge seen in Fig. 5(a). The collocation of a ridge perfectly aligned along a step edge suggests that the graphene layers located at step edges contain a number of atomic-scale defects which seed buckling under the compressive stress of cooling.

The formation of ridges in turn causes a rotation in the top layer(s) of the FLG, resulting in a moiré superlattice. We estimate that moiré regions are found near ridges in about 20% of our images. Moiré regions are never found as isolated regions surrounded by flat graphene layers. Moiré regions are common on FLG samples grown at 1500 °C, rare on 1550 °C samples, and never found on 1600 °C samples. The ridges, next to which the moiré regions are usually found, have high aspect ratios at 1500 °C but are smoother and more rounded at 1600 °C. These observations suggest that high stresses in the graphene layer, which are proportional to the aspect ratio of the ridges, can produce localized rotation of graphene layers.

It is possible that the moiré superlattices form when two disparate growth regions of graphene layers merge and overlap. If this is the explanation for the 2D moiré superlattices, then the likelihood of finding a moiré region would be roughly the same as the number density of graphene seed

regions. However, we find that the moiré regions are the exception, not the norm, suggesting that they are produced by a relatively rare set of circumstances.

It is possible that the moiré superlattices form when graphene growth encounters a SiC step edge. If, for example, the graphene growing on the top terrace has a different rotation from that growing on the lower terrace, then the growth of an overlayer across a step edge could cause a moiré superlattice to form. However, graphene growth near many of the step edges in FLG exhibits a standard Bernal stacking, with no evidence for a moiré superlattice. Also, it is possible to find examples (see Fig. 7) that indicate graphene growth must be commensurate *across* both upper and lower terraces to account for the same periodicity and orientation of the moiré superlattice on both sides of a step edge. These observations all argue against overlayer growth as a possible cause of the moiré superlattices.

It is also possible that atomic-scale defects in the graphene layers, such as the formation of pentagonal-heptagonal defects, nucleate a moiré superlattice. It is well established that a pentagonal-heptagonal defect produces a localized upward puckering of the graphene layer, accompanied by a rotation of the graphene lattice. As a result, the graphene lattice would be highly rotated near the pentagonal-heptagonal defect and would relax to an undeformed lattice as a function of distance from the defect. The resulting moiré superlattice formed by the growth of a pristine graphene layer over such a pentagonal-heptagonal defect would have a radially varying periodicity, similar to that around a screw dislocation. The moiré superlattices found in our STM study all have a constant periodicity across their entire area, eliminating the possibility that they are formed by localized pentagonal-heptagonal defects.

Since there is sufficient thermal energy at the growth temperature to anneal any moiré superlattices that might develop during growth, we believe that the 2D moiré superlattices in FLG must be produced during the formation of ridges upon cooling. The ridge formation evidently causes a relative rotation between different graphene layers.

VII. CONCLUSIONS

Studies to characterize few-layer graphene (FLG) formed on $4H$-SiC$(000\bar{1})$ substrates have been summarized. FLG grown at temperatures ranging between 1475 and 1600 °C have been investigated. In our study, we confined our attention to FLG that was grown during a 10 min time interval at the specified growth temperature.

Both x-ray photoelectron spectroscopy (XPS) and scanning tunneling microscopy (STM) were used to characterize the quality of the FLG surface. The XPS studies were useful in confirming the graphitic composition and estimating the thickness of the FLG layers. STM studies revealed a wide variety of different nanometer-scale features on the FLG surface which include rough graphene, atomically smooth graphene, 1D grain boundaries, 1D ridges, and 2D moiré superlattices.

Our efforts to understand the origin of these varied features provide considerable insights into the relevant growth mechanisms of FLG on $4H$-SiC$(000\bar{1})$ substrates. In general, our data are qualitatively consistent with a carpetlike growth mechanism of FLG, in which select nanofacets on SiC step edges rapidly produce excess C atoms which diffuse across the substrate to form graphene layers. Upon cooling, the graphene layers are subject to a compressive thermal stress which causes the FLG to fold and buckle along lines of defects that are weak points in the graphene layers. This buckling produces ripples and ridges which induce local strain fields that occasionally cause a rotation of the graphene layers, forming 2D moiré superlattices. The additional periodicity imposed on the electron states in FLG supporting a superlattice will create many narrow minibands separated by small energy minigaps. The creation of these minibands has important implications, especially with regard to increased electron scattering and optical absorption in superlattice regions of FLG.

ACKNOWLEDGMENTS

This research was supported by an Indiana 21st Century Fund. L.B. was supported by Sandia National Laboratories' Excellence in Science and Engineering program. The authors gratefully acknowledge J. Appenzeller, J. Cooper, and T. Sands for many helpful comments during the course of this work.

[1] A. Cresti, N. Nemec, B. Biel, G. Niebler, F. Triozon, G. Cuniberti, and S. Roche, Nano Res. **1**, 361 (2008).
[2] K. Yamashita, M. Saito, and T. Oda, Jpn. J. Appl. Phys., Part 2 **45**, 6534 (2006).
[3] P. Simonis, C. Goffaux, P. A. Thiry, L. P. Biro, P. Lambin, and V. Meunier, Surf. Sci. **511**, 319 (2002).
[4] L. Porte, C. H. Devilleneuve, and M. Phaner, J. Vac. Sci. Technol. B **9**, 1064 (1991).
[5] B. K. Annis, D. F. Pedraza, and S. P. Withrow, J. Mater. Res. **8**, 2587 (1993).
[6] R. H. Telling, C. P. Ewels, A. A. El-Barbary, and M. I. Heggie, Nature Mater. **2**, 333 (2003).
[7] G. M. Rutter, J. N. Crain, N. P. Guisinger, T. Li, P. N. First, and J. A. Stroscio, Science **317**, 219 (2007).
[8] N. P. Guisinger, G. M. Rutter, J. N. Crain, C. Heiliger, P. N. First, and J. A. Stroscio, J. Vac. Sci. Technol. A **26**, 932 (2008).
[9] K. Kojima, T. Suzuki, S. Kuroda, J. Nishio, and K. Arai, Jpn. J. Appl. Phys., Part 2 **42**, L637 (2003).
[10] S. R. Snyder, T. Foecke, H. S. White, and W. W. Gerberich, J. Mater. Res. **7**, 341 (1992).
[11] H. Hiura, J. Mater. Res. **16**, 1287 (2001).
[12] H. A. Mizes and J. S. Foster, Science **244**, 559 (1989).
[13] K. F. Kelly, D. Sarkar, G. D. Hale, S. J. Oldenburg, and N. J. Halas, Science **273**, 1371 (1996).

[14] J. Cervenka and C. F. J. Flipse, J. Phys.: Conf. Ser. **61**, 190 (2007).
[15] M. Kuwabara, D. R. Clarke, and D. A. Smith, Appl. Phys. Lett. **56**, 2396 (1990).
[16] Z. Y. Rong and P. Kuiper, Phys. Rev. B **48**, 17427 (1993).
[17] W. T. Pong and C. Durkan, J. Phys. D **38**, R329 (2005).
[18] H. Beyer, M. Muller, and T. Schimmel, Appl. Phys. A: Mater. Sci. Process. **68**, 163 (1999).
[19] F. Varchon, P. Mallet, L. Magaud, and J. Y. Veuillen, Phys. Rev. B **77**, 165415 (2008).
[20] F. Owman and P. Martensson, Surf. Sci. **369**, 126 (1996).
[21] A. Charrier, A. Coati, T. Argunova, F. Thibaudau, Y. Garreau, R. Pinchaux, I. Forbeaux, J. M. Debever, M. Sauvage-Simkin, and J. M. Themlin, J. Appl. Phys. **92**, 2479 (2002).
[22] W. Chen, H. Xu, L. Liu, X. Gao, D. Qi, G. Peng, S. C. Tan, Y. Feng, K. P. Loh, and A. T. S. We, Surf. Sci. **596**, 176 (2005).
[23] C. Berger *et al.*, Science **312**, 1191 (2006).
[24] V. W. Brar, Y. Zhang, Y. Yayon, T. Ohta, J. L. McChesney, A. Bostwick, E. Rotenberg, K. Horn, and M. F. Crommie, Appl. Phys. Lett. **91**, 122102 (2007).
[25] C. Riedl, U. Starke, J. Bernhardt, M. Franke, and K. Heinz, Phys. Rev. B **76**, 245406 (2007).
[26] P. Lauffer, K. V. Emtsev, R. Graupner, T. Seyller, L. Ley, S. A. Reshanov, and H. B. Weber, Phys. Rev. B **77**, 155426 (2008).
[27] P. Mallet, F. Varchon, C. Naud, L. Magaud, C. Berger, and J. Y. Veuillen, Phys. Rev. B **76**, 041403(R) (2007).
[28] A. J. Vanbommel, J. E. Crombeen, and A. Vantooren, Surf. Sci. **48**, 463 (1975).
[29] I. Forbeaux, J. M. Themlin, and J. M. Debever, Surf. Sci. **442**, 9 (1999).
[30] I. Forbeaux, J. M. Themlin, A. Charrier, F. Thibaudau, and J. M. Debever, Appl. Surf. Sci. **162-163**, 406 (2000).
[31] T. Angot, M. Portail, I. Forbeaux, and J. M. Layet, Surf. Sci. **502-503**, 81 (2002).
[32] J. Hass, F. Varchon, J. E. Millan-Otoya, M. Sprinkle, N. Sharma, W. A. de Heer, C. Berger, P. N. First, L. Magaud, and E. H. Conrad, Phys. Rev. Lett. **100**, 125504 (2008).
[33] J. Coraux, A. T. N'Diaye, C. Busse, and T. Michely, Nano Lett. **8**, 565 (2008).
[34] A. N. Obraztsov, E. A. Obraztsova, A. V. Tyurnina, and A. A. Zolotukhin, Carbon **45**, 2017 (2007).
[35] B. Wang, M. L. Bocquet, S. Marchini, S. Gunther, and J. Wintterlin, Phys. Chem. Chem. Phys. **10**, 3530 (2008).
[36] M. Sasaki, Y. Yamada, Y. Ogiwara, S. Yagyu, and S. Yamamoto, Phys. Rev. B **61**, 15653 (2000).
[37] J. M. Campanera, G. Savini, I. Suarez-Martinez, and M. I. Heggie, Phys. Rev. B **75**, 235449 (2007).
[38] Y. Q. Wu *et al.*, Appl. Phys. Lett. **92**, 092102 (2008).
[39] E. Rollings, G. H. Gweon, S. Y. Zhou, B. S. Mun, J. L. McChesney, B. S. Hussain, A. Fedorov, P. N. First, W. A. de Heer, and A. Lanzara, J. Phys. Chem. Solids **67**, 2172 (2006).
[40] I. Horcas, R. Fernandez, J. M. Gomez-Rodriguez, J. Colchero, J. Gomez-Herrero, and A. M. Baro, Rev. Sci. Instrum. **78**, 013705 (2007).
[41] L. I. Johansson, F. Owman, and P. Martensson, Phys. Rev. B **53**, 13793 (1996).
[42] L. Muehlhoff, W. J. Choyke, M. J. Bozack, and J. T. Yates, J. Appl. Phys. **60**, 2842 (1986).
[43] D. Briggs and J. Grant, *Surface Analysis by Auger and X-ray Photoelectron Spectroscopy* (IM Publications and SurfaceSpectra Limited, Chichester, UK, 2003).
[44] C. S. Fadley, *Basic Concepts of X-ray Photoelectron Spectroscopy*, Electron Spectroscopy: Theory, Techniques, and Applications Vol. 2 (Academic, New York, 1978).
[45] NIST SRD-82, National Institute of Standards and Technology, Gaithersburg, MD, 2001.
[46] See EPAPS Document No. E-PRBMDO-79-039908 for the derivation of Eq. (3) and the thickness calculation for the sample grown at 1500 °C. For more information on EPAPS, see http://www.aip.org/pubservs/epaps.html.
[47] G. Prakash, M. Capano, M. Bolen, D. Zemlyanov, and R. Reifenberger (unpublished).
[48] M. Grodzicki, P. Mazur, S. Zuber, G. Urbanik, and A. Ciszewski, Thin Solid Films **516**, 7530 (2008).
[49] C. Gackenheimer, L. Cayón, and R. Reifenberger, Ultramicroscopy **106**, 389 (2006).
[50] T. Seyller *et al.*, Surf. Sci. **600**, 3906 (2006).
[51] J. C. Meyer, A. K. Geim, M. I. Katsnelson, K. S. Novoselov, T. J. Booth, and S. Roth, Nature (London) **446**, 60 (2007).
[52] E. Stolyarova, K. T. Rim, S. M. Ryu, J. Maultzsch, P. Kim, L. E. Brus, T. F. Heinz, M. S. Hybertsen, and G. W. Flynn, Proc. Natl. Acad. Sci. U.S.A. **104**, 9209 (2007).
[53] M. Ishigami, J. H. Chen, W. G. Cullen, M. S. Fuhrer, and E. D. Williams, Nano Lett. **7**, 1643 (2007).
[54] F. de Juan, A. Cortijo, and M. A. H. Vozmediano, Phys. Rev. B **76**, 165409 (2007).
[55] L. Brey and J. J. Palacios, Phys. Rev. B **77**, 041403(R) (2008).
[56] F. Guinea, M. I. Katsnelson, and M. A. H. Vozmediano, Phys. Rev. B **77**, 075422 (2008).
[57] N. D. Mermin, Phys. Rev. **176**, 250 (1968).
[58] S. V. Morozov, K. S. Novoselov, M. I. Katsnelson, F. Schedin, L. A. Ponomarenko, D. Jiang, and A. K. Geim, Phys. Rev. Lett. **97**, 016801 (2006).
[59] D. D. Quinn, J. P. Wilber, C. B. Clemons, G. W. Young, and A. Buldum, Int. J. Non-Linear Mech. **42**, 681 (2007).
[60] J. P. Wilber, C. B. Clemons, G. W. Young, A. Buldum, and D. D. Quinn, Phys. Rev. B **75**, 045418 (2007).
[61] A. K. Geim and K. S. Novoselov, Nature Mater. **6**, 183 (2007).
[62] A. Fasolino, J. H. Los, and M. I. Katsnelson, Nature Mater. **6**, 858 (2007).
[63] J. M. Carlsson, Nature Mater. **6**, 801 (2007).
[64] A. Golz, G. Horstmann, E. S. von Kamienski, and H. Kurz, in International Conference on Silicon Carbide and Related Materials 1995 (ICSCRM-95), edited by S. Nakashima, H. Matsunami, S. Yoshida, and H. Harima (Inst. Phys. Conf. Ser. No. 142, Kyoto, Japan, 1995), p. 633.